Global Biogeochemical Cycles®

RESEARCH ARTICLE
10.1029/2021GB006964

Large Methane Emissions From the Pantanal During Rising Water-Levels Revealed by Regularly Measured Lower Troposphere CH_4 Profiles

M. Gloor[1], L. V. Gatti[2], C. Wilson[3,4], R. J. Parker[5,6], H. Boesch[5,6], E. Popa[7], M. P. Chipperfield[3,4], B. Poulter[8], Z. Zhang[8], L. Basso[2], J. Miller[9], J. McNorton[10], C. Jimenez[11], and C. Prigent[11]

[1]School of Geography, University of Leeds, Leeds, UK, [2]National Institute for Space Research (INPE), Earth System Science Center (CCST), Greenhouse Gases Laboratory (LaGEE), Jose dos Campos, Brazil, [3]National Centre for Earth Observation, University of Leeds, Leeds, UK, [4]School of Earth and Environment, University of Leeds, Leeds, UK, [5]National Centre for Earth Observation, University of Leicester, Leicester, UK, [6]Earth Observation Science, School of Physics and Astronomy, University of Leicester, Leicester, UK, [7]Universiteit Utrecht, Utrecht, The Netherlands, [8]Department of Geographical Sciences, University of Maryland, College Park, MD, USA, [9]Global Monitoring Division, Earth System Research Laboratory, National Oceanic and Atmospheric Administration, Boulder, CO, USA, [10]European Centre for Medium-Range Weather Forecasts, Reading, UK, [11]Observatoire de Paris, Paris, France

Key Points:

- Large CH_4 boundary layer-free troposphere differences over Pantanal wetlands revealed by vertical atmospheric CH_4 profile data
- According to atmospheric data, CH_4 flux is large during the early expansion phase of the inundated area and weakens at peak extent
- Prognostic global wetlands CH_4 emission models have limited skill regarding seasonality of Pantanal emissions

Supporting Information:

Supporting Information may be found in the online version of this article.

Correspondence to:

M. Gloor,
eugloor@gmail.com

Citation:

Gloor, M., Gatti, L. V., Wilson, C., Parker, R. J., Boesch, H., Popa, E., et al. (2021). Large methane emissions from the Pantanal during rising water-levels revealed by regularly measured lower troposphere CH_4 profiles. *Global Biogeochemical Cycles*, *35*, e2021GB006964. https://doi.org/10.1029/2021GB006964

Received 31 JAN 2021
Accepted 13 SEP 2021

Abstract

The Pantanal region of Brazil is the largest seasonally flooded tropical grassland and, according to local chamber measurements, a substantial CH_4 source. CH_4 emissions from wetlands have recently become of heightened interest because global atmospheric $^{13}CH_4$ data indicate they may contribute to the resumption of atmospheric CH_4 growth since 2007. We have regularly measured vertical atmospheric profiles for 2 years in the center of the Pantanal with the objectives to obtain an estimate of CH_4 emissions using an atmospheric approach, and provide information about flux seasonality and its relation to controlling factors. Boundary layer-free troposphere differences observed in the Pantanal are large compared to other wetlands. Total emissions based on a planetary boundary layer budgeting technique are 2.0–2.8 $TgCH_4\ yr^{-1}$ (maximum flux ~0.4 $gCH_4\ m^{-2}\ d^{-1}$) while those based on a Bayesian inversion using an atmospheric transport model are ~3.3 $TgCH_4\ yr^{-1}$. Compared to recent estimates for Amazonia (~41 ± 3 $TgCH_4\ yr^{-1}$, maximum flux ~0.3 $gCH_4\ m^{-2}\ d^{-1}$) these emissions are not that large. Our Pantanal data suggest a clear flux seasonality with CH_4 being released in large amounts just after water levels begin to rise again after minimum levels have been reached. CH_4 emissions decline substantially once the maximum water level has been reached. While predictions with prognostic wetland CH_4 emission models agree well with the magnitude of the fluxes, they disagree with the phasing. Our approach shows promise for detecting and understanding longer-term trends in CH_4 emissions and the potential for future wetlands CH_4 emissions climate feedbacks.

Plain Language Summary

CH_4 emissions contribute substantially to greenhouse warming and atmospheric concentrations continue to grow rapidly. Increases in emissions from wetlands may contribute. We have measured regularly vertical CH_4 concentration profiles over the Pantanal, the largest tropical seasonally flooded grasslands, to provide an estimate of these emissions and to determine seasonal cycle. Our estimates are similar to earlier estimates based on direct flux measurements on the ground. Fluxes vary strongly seasonally. They are largest during the rise of water levels and decrease before maximum levels have been reached. Our data show that longer-term vertical profile measurements could provide an answer whether wetland emissions are changing.

1. Introduction

Methane is one of the main contributors to the anthropogenic perturbation of the Earth's surface radiation budget caused by increasing the atmospheric burden of greenhouse gases. Compared to preindustrial levels atmospheric CH_4 concentrations have nearly tripled. Although the anthropogenic atmospheric CH_4 concentration perturbation (in units of molar ratio) is currently approximately 100 times smaller than the carbon dioxide (CO_2) perturbation (e.g., MacFarling et al., 2006) it contributes approximately 20% to the anthropogenically caused global warming (IPCC Report, 2014). The continued increase in atmospheric

methane is thus a major concern. Unlike CO_2, CH_4 undergoes chemical reactions in the troposphere, primarily oxidation by OH radicals (Cicerone & Oremland, 1988; Levy, 1971), one of the reasons why CH_4 levels in the troposphere are lower than CO_2 levels. Methane sources can be categorized into natural and anthropogenic sources (e.g., Saunois et al., 2016, 2020). The main anthropogenic sources include emissions resulting from agriculture and waste (~35% of total emissions), oil, coal and gas production (~20%), and biomass burning (~6%). Production and emission of methane from wetlands is the primary natural source, estimated to account currently for approximately 30% of the total (Saunois et al., 2016, 2020). Production of methane in wetlands is the result of anaerobic respiration of organic carbon compounds by methanogens under specific pH and redox conditions (e.g., Baker-Blocker et al., 1977; Bridgham et al., 2013). Partitioning the atmospheric methane budget into emission sectors remains a challenge (e.g., Saunois et al., 2020). Indeed, controls on neither decadal-scale nor interannual variations of atmospheric methane are fully understood. For example, a well-known feature of the atmospheric methane record is a period starting in 1990 when atmospheric methane concentrations seemed to start to level off toward a constant value around 2006, suggesting a stationary state may have been reached (Dlugokencky et al., 1998). However, the growth abruptly resumed in 2007 and rebounded to a similar or faster growth to that of the 1980s. In contrast to previous growth periods, the resumption of the atmospheric CH_4 growth rate in 2007 was associated with atmospheric $\delta^{13}CH_4$, the fraction of atmospheric methane containing carbon-13 instead of carbon-12, which started to decrease. Despite this additional isotopic fingerprint, the cause for resumed growth has not yet been fully attributed to changes in source sectors. Nonetheless, the decreasing trend in $\delta^{13}CH_4$ raises the possibility of a wetland emission-climate feedback (e.g., caused by increased precipitation, warming, or increases in biomass production) (Nisbet et al., 2016). Indeed, occurrences of large floods have increased in Bolivia which contains the Llanos de Moxos seasonally flooded wetlands, the contrast between wet and dry season precipitation in Amazonia has increased and substantial parts of tropical South America have experienced particularly rapid surface air temperature warming rates (Barichivich et al., 2018; Gloor et al., 2018; Jiménez-Muñoz et al., 2013; Ovando et al., 2015). Furthermore, unlike for CO_2, ENSO (El Niño-Southern Oscillation) climate variations do not have a directly visible influence on interannual variation of the atmospheric CH_4 growth rate, another aspect of the global CH_4 cycle which is also not fully understood. Because of the large contribution of total CH_4 emissions from wetlands, changes of these emissions may indeed have possibly contributed to the resumption of atmospheric CH_4 inventory growth. A substantial fraction of global wetlands is located in the tropics (e.g., Keddy et al., 2009). They host several major seasonally flooded savannahs as well as major seasonally flooded floodplains of large rivers like the Amazon, the Paraná, and the Congo Rivers. In South America, major seasonally flooded savannahs include the Llanos de Moxos (Bolivia), the Orinoco savannahs (Venezuela), and the Pantanal (Brazil), of which the Pantanal is the largest (estimates of its area range from 140,000 to 180,000 km^2, e.g., Diegues, 1994; Hamilton et al., 2002; Junk et al., 2014; Keddy et al., 2009) (Figure 1).

Given this background, and as part of a larger recent effort by a UK-funded consortium (MOYA, "Methane Observations and Yearly Assessments") to obtain improved tropical wetland CH_4 emissions, we report here results obtained from atmospheric concentration measurements over the Pantanal. Our approach takes advantage of the flux-integrating nature of the planetary boundary layer (PBL), which is the result of strong mixing caused by near-surface turbulence, but slow air exchange between the boundary layer and the free troposphere. Surface-to-atmosphere gas fluxes accumulate along air parcel trajectories, initially primarily in the PBL (height above ground on the order of 2 km) (e.g., Chou et al., 2002), causing distinct concentration differences between the PBL and the free troposphere. This signal is representative for fluxes from a large area. The area should scale roughly with the square of the air-mass trajectory path length over a timescale of the exchange time between the PBL and the free troposphere (a length scale of a few hundred kilometers).

The measurements presented here complement earlier CH_4 flux estimates for several subregions of the Pantanal based on flux chamber measurements (Hamilton et al., 1995; Marani & Alvala, 2007) with a large-scale integrating atmospheric approach. Besides providing an integral estimate of CH_4 flux from the Pantanal, we aim to characterize the time-variation of fluxes and thus contribute to understanding of some of the controls of CH_4 fluxes. Measurements consist of vertical CH_4 profiles up to 4.4 km height measured roughly every month over a period of approximately 2 years, thus covering nearly two full seasonal cycles. Using these data, we estimate fluxes with a variation of the traditional air-column budgeting technique and a global inverse model of 3-D atmospheric transport. To put the flux data into a longer-term context, and to

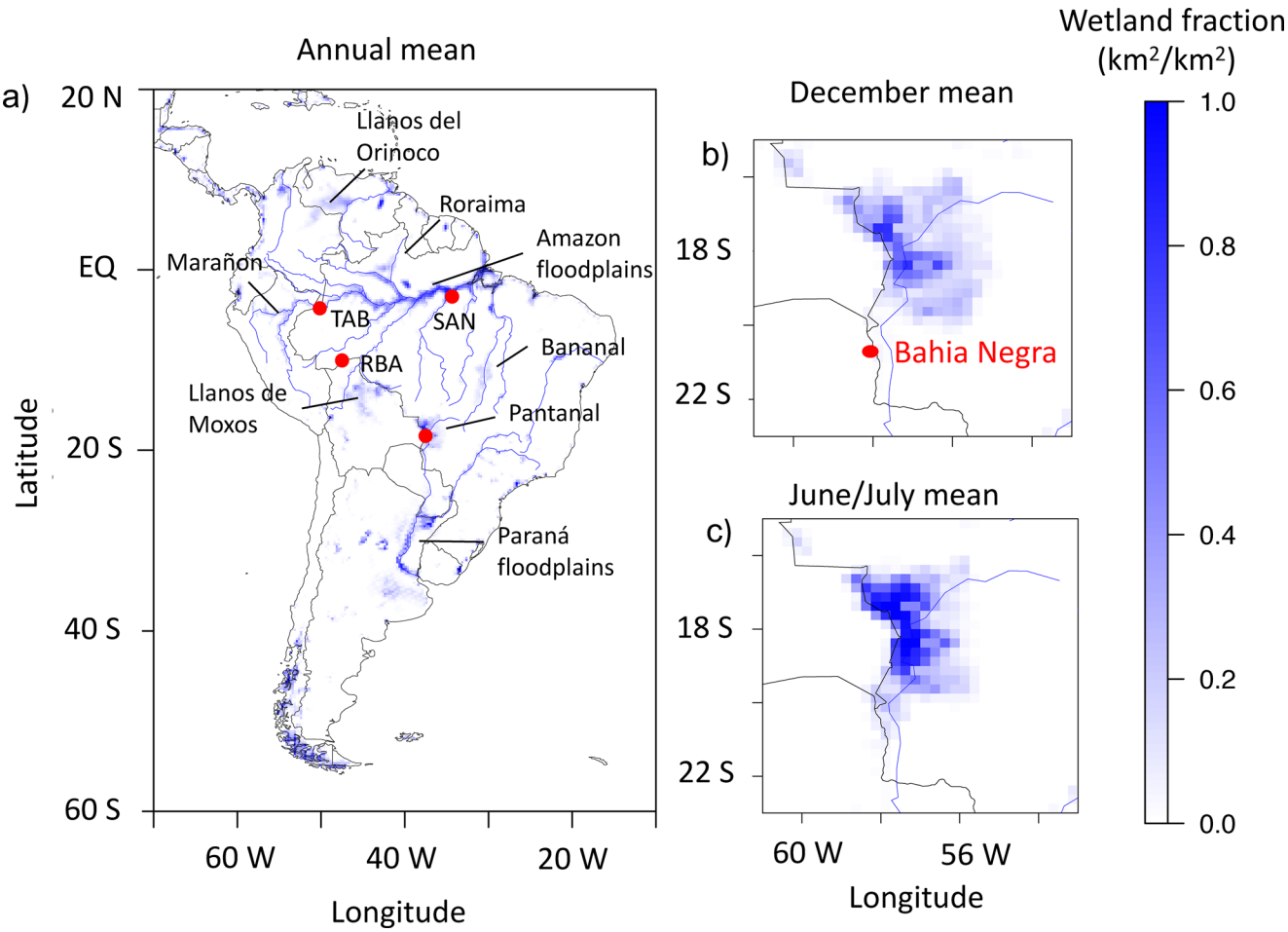

Figure 1. (a) Annual mean wetland fraction estimated using remote sensing data (Prigent et al., 2020) which reveal the major South American wetlands. The map also includes the sites where CH_4 profile data have been measured regularly and which are used in this study: TAB (Tabatinga), RBA (Rio Branco), SAN (Santarem), and Pantanal, (b) wetland fraction in the Pantanal during low water (December) and the Paraguay River stage site at Bahia Negra, and (c) during high water levels (June/July).

help understand the emission seasonality and process, we also use estimates of water levels, burned area and air-column CH_4 estimates obtained based on reflectance data measured on the GOSAT satellite. Finally, we compare our results with predictions with wetland CH_4 emissions models and assess what they may imply for wetland emissions modeling.

2. Methods

2.1. Study Region

The Pantanal region is an extraordinarily flat, low-elevation (~100 m above sea level) plain located centrally in South America, to the south of the Amazon basin (Figure 1). It is a sedimentary basin in a tectonic depression (Assine et al., 2004). The plain is surrounded by a half-circle-shaped mountain range stretching north-east-south around the basin while it is not bordered by mountains to the west. The headwaters of the Paraguay River are located in the Pantanal. Further downstream, the Paraguay River joins the Paraná River which in turn enters the Atlantic Ocean in Buenos Aires. The Pantanal is seasonally flooded (e.g., Alho et al., 2012). This flood rhythm reflects the strong seasonality of precipitation in the highlands north-east of the Pantanal, the waters of which drain into the Pantanal. Precipitation in the Pantanal itself has also a strong seasonal cycle. Rain starts in September with rainfall on the order of 50 mm mo^{-1}. It peaks around January to February with approximately 200 mm mo^{-1}, while there is almost no rain during June to August

(e.g., Ivory et al., 2019). Flooding of the region lags peak precipitation by close to half a year with peak flooding occurring typically around July (e.g., Figure 3c). Vegetation of the Pantanal can be characterized as follows (Evans et al., 2014): The wide gently westward sloping fan to the east of the Paraguay River, the main water stem of the Pantanal, is covered by "open wood savannah" (grassland interspersed with trees) (approximately 50% of the Pantanal by area) (Figures 1b and 1c). Then, along the Paraguay River, land cover is swampy mixed savannah and grasslands, and open water (approximately 20% by area) (Figures 1b and 1c). Woodlands occur primarily in the north-east and, together with riparian forests, cover roughly 14% of Pantanal's area. Finally, agriculturally used land located mainly at the eastern fringes account for 6% by area (Evans et al., 2014).

Water movement in the Pantanal is slow and oxygen levels are often very low. Based on numerous measurements, the low oxygen levels have been attributed to respiration of aquatic vascular plant material (Hamilton et al., 1995). These measurements also revealed seasonally highly supersaturated CH_4 levels in the water column attributed to influx of methane from the sediments produced by methanogenesis (Hamilton et al., 1995).

Population density in the Pantanal is low (Schulz et al., 2019). During the driest part of the year and the beginning of the wet season there is a strong increase in fires. Fires typically start in the middle of the dry season (July) and peak in September. From December onwards fire frequency returns to very low values as seen, for example, by fire counts measured by the Moderate Resolution Imaging Spectroradiometer (MODIS) (Boschetti et al., 2019; Giglio et al., 2018).

One aspect of the Pantanal is that CH_4 emissions are potentially not well represented in current prognostic global wetland CH_4 emission models. This is a consequence of its very flat topography. Existing prognostic models predict flooded area based on terrain slope ("topographic index," TOPMODEL, Beven & Kirkby, 1979) and assume that the hydraulic gradient is proportional to terrain slope (JULES land surface model, Gedney & Cox, 2003; Lund-Potsdam-Jena model-*wsl* version (LPJ-wsl), Zhang et al., 2016). This last assumption is not correct if topography is quite flat (personal comm. Mike Kirkby).

2.2. Regular Vertical Profile Sampling of Lower Troposphere CH_4, CO, and CO_2 Using Small Aircraft

To determine CH_4 fluxes from the Pantanal region, we have measured vertical CH_4 dry air mole fraction profiles on roughly a monthly basis using small aircraft. The profiles extend from near the ground to approximately 4.4 km altitude. Sampling was performed using an array of flasks, integrated into a suitcase, which were filled sequentially during aircraft descent with valves being opened and closed by a programmable microcontroller. Typically, 17 flasks were filled for each profile with approximately 200 m vertical distance between each sample (Figure S2). The suitcase with the flasks was then sent to the high precision Greenhouse Gas analysis laboratory (LAGEE) at INPE (Instituto Nacional de Pesquisas Espaciais) at Sao Jose dos Campos, Brazil. At LAGEE dry air mole fractions of CO_2, CH_4, and carbon monoxide (CO) of flask air were determined relative to World Meteorological Organization calibration scales. We started the measurements on March 3, 2017 and the last profile was taken on September 30, 2019. The vertical profile samples were all taken during midday over the center of the Pantanal (approximate coordinates 19.45°S, 56.4°W). To reach this point, a small aircraft flew from Campo Grande to the center of the Pantanal (distance approximately 240 km in north-westerly direction). It then descended from 4.4 km altitude above ground to 0.3 km before returning back to Campo Grande. On one return flight, we additionally filled a sequence of air flasks all the way back to Campo Grande permitting a limited assessment of the horizontal extent of CH_4 elevations in the PBL above the Pantanal.

2.3. Atmospheric Column CH_4 Estimates Based on Reflectance Data Measured by a Fourier-Transform Spectrometer in the Shortwave Infrared on the GOSAT Satellite

To corroborate results obtained from the vertical profile data, we also use whole air-column CH_4 estimated from space by instruments on the GOSAT satellite (Kuze et al., 2009). Whole-air-column CH_4 is derived from radiance differences of sunlight traversing the atmosphere twice versus light directly received by the sensor on the satellite using the approach of Frankenberg et al. (2005). The method estimates the CH_4/CO_2

ratio instead of CH_4 alone to minimize systematic errors, which are assumed to affect both CH_4 and CO_2 absorption along the light path and thus largely cancel each other. The method needs an independent estimate of whole column CO_2 to convert the CH_4/CO_2 ratio to atmospheric column CH_4. Whole-air-column CO_2 is estimated using transport model simulations of atmospheric CO_2 using realistic CO_2 surface fluxes. A quantitative comparison of retrievals with in situ vertical profile air concentration data at the three Amazonian sites in Figure 1a of Webb et al. (2016) revealed good agreement of the column retrievals and the in situ data. A detailed description of method and data are given in Parker et al. (2011, 2020). This study uses Version 7.2 of the University of Leicester GOSAT Proxy XCH_4.

2.4. Flux Estimation Using Atmospheric Air-Column Budget

We exploit PBL versus free troposphere CH_4 differences to obtain flux estimates. Assuming well-mixed conditions in the PBL and that exchange of air between the PBL and free troposphere can be described by an air exchange rate Q ($m^3\ m^{-2}\ h^{-1}$), the time rate of change of mean PBL dry air mole fraction is given by

$$\frac{\partial \overline{\chi}_{PBL}}{\partial t} = \frac{1}{\overline{n} \cdot h} \cdot F_{srf} - \frac{1}{\tau} \cdot \left(\overline{\chi}_{PBL} - \chi_{free\ trop} \right) - u \frac{\partial \overline{\chi}_{PBL}}{\partial x}$$

with

$$\overline{\chi}_{PBL} \equiv \frac{\frac{1}{h}\int_0^h X \cdot n\, dz}{\frac{1}{h}\int_0^h n\, dz}, \overline{n} \equiv \frac{1}{h}\int_0^h n\, dz, \tau \equiv \frac{h}{Q}.$$

Here χ is dry air molar ratio, $\overline{\chi}_{PBL}$and $\chi_{free\ trop}$ are dry air mole fraction in the PBL and in the free troposphere, respectively, t time (h), h PBL height (m), n air molar density (mol m^{-3}), F_{srf} flux to the atmosphere (mol $m^{-2}\ h^{-1}$), z vertical coordinate (m), u wind velocity (m h^{-1}), and $\overline{\ }$ indicates a PBL average (Chou et al., 2002). The main sink, oxidation by OH, over typical boundary layer free troposphere air exchange timescales τ, is negligible. When evaluating this equation on monthly time steps the derivatives of $\chi_{free\ trop}$ are small compared to derivatives of $\overline{\chi}_{PBL}$. Thus, the equation can be reformulated for PBL mean free troposphere (>3,000 m above ground) differences $\Delta\chi \equiv \overline{\chi}_{PBL} - \chi_{free\ trop}$ and solved for surface flux F_{srf} to yield

$$F_{srf} = \overline{n} \cdot h \cdot \left\{ \frac{\partial \Delta\chi}{\partial t} + \frac{\Delta\chi}{\tau} + \overline{u} \frac{\partial \Delta\chi}{\partial x} \right\} \quad (1)$$

(a detailed derivation is provided in the Supporting Information S1). The first term in parentheses on the right of Equation 1 tends to be small compared to the other two terms. Thus, given an estimate of PBL-free troposphere air exchange time τ, PBL-average wind speed and PBL-free troposphere difference and its large-scale gradient, then the surface flux can be estimated. We estimate here the large-scale gradient $\frac{\partial \Delta\chi}{\partial x}$ from the GOSAT retrievals (PBL-free troposphere differences decline to 0 over a spatial scale of ~700 km downwind, Figure S4). For our approach to hold, it is also necessary that the PBL-free troposphere differences are caused by fluxes from the region in question and not advected from remote regions where there are large CH_4 fluxes, such as the Amazon.

2.5. Flux Estimation Using Inverse Modeling of 3-D Atmospheric Transport

We also use the variational inverse model INVICAT (Wilson et al., 2014) based on TOMCAT, a global 3-D Eulerian atmospheric transport and chemistry model (Chipperfield, 2006; Monks et al., 2018) for flux estimation. Fluxes are estimated by minimizing the sum of the mismatch between uncertainty-weighted observed and simulated atmospheric trace gas mixing ratios, here CH_4, and simultaneously between prior and posterior CH_4 fluxes. The data assimilated include CH_4 retrievals based on radiances measured by instruments on GOSAT as described above (Parker et al., 2018, 2020), in situ measured CH_4 mole fractions at the surface station network operated by NOAA Global Monitoring Laboratory and the CH_4 mole fraction data measured at the center of the Pantanal. The set of prior guess flux emissions are described in detail in Wilson et al. (2021) as well as in the Supporting Information S1. The spatial resolution of the model is 5.6° × 5.6° which is quite coarse but sufficient for this study.

2.6. Inundated Area

We use the GIEMS (Global Inundation Extent from Multisatellites) estimates of inundated area of Prigent et al. (2020). Existing estimates, which cover the period from January 1992 to December 2015, have been complemented for the Pantanal region by the data for the years 2016–2018 for this study. For technical reasons similar estimates for 2019 cannot yet be obtained. Fraction of inundated area is estimated monthly with 0.25° × 0.25° spatial resolution. Identification of wetland area is based on passive microwave radiation (difference between vertically and horizontally polarized radiation), active microwave backscattering (backscattering coefficient) and near-infrared reflectance (via NDVI, normalized difference vegetation index) (Prigent et al., 2020).

2.7. River Stage Height

As an indicator of flood levels during 2019 and 2020, when GIEMS inundated area estimates are not available, we use here river stage records measured at Bahia Negra (Figure 1) by ANA (Agencia Nacional de Aguas e Saneamento Basico, Brazilian Hydrological Service).

2.8. Burned Area

As a proxy for CH_4 emitted by biomass burning, we use burned area estimates based on data measured by MODIS on the Terra and Aqua satellites (Boschetti et al., 2019; Giglio et al., 2018). Briefly, the algorithm uses vegetation index changes over time to identify burned areas and corroborate fires as the cause with fire spots measured by remote sensing from temperature anomalies. The accuracy of the burned area estimator has been assessed in various ways, including comparisons with manually interpreted Landsat images (Giglio et al., 2018). While the estimator misses approximately 25% of fires, this is unlikely to affect assessment of interannual variation for which it is used in this study (Giglio et al., 2018).

2.9. Global Wetland Model CH_4 Flux Predictions

Our results are potentially of interest for prognostic wetland CH_4 emissions models used to analyze global atmospheric CH_4 patterns in space and time and also as components of Earth system models. Here we use predictions of the LPJ-wsl dynamic global vegetation model, developed for carbon cycle applications based on the original LPJ global vegetation model (Sitch et al., 2003). LPJ-wsl models surface inundation using the overland flow hydrological TOPMODEL (Beven & Kirkby, 1979; Zhang et al., 2016), which is used in a prognostic wetland CH_4 emission model (Zhang et al., 2018). The wetland CH_4 emissions component uses daily climate fields aggregated from 1-hourly reanalysis MERRA2 (Modern-Era retrospective analysis for Research and Applications Version 2) from the NASA Global Modeling and Data Assimilation Office (Gelaro et al., 2017). We also use a version of the JULES model (McNorton et al., 2016).

3. Results

To help interpret the atmospheric CH_4 concentration data, we use two indicators of water levels: inundated area extent estimated with remote sensing (GIEMS) and measurements of Paraguay River stage levels. The records agree fairly well with regards to seasonality (phasing) and to some extent with regards to interannual variation (Figure 2). We therefore use the stage level record as an indicator of the temporal course of flood levels in 2019/2020 when inundated area extent data from remote sensing are missing. The records indicate that flood levels during the period of CH_4 measurements were average in 2017 and high in 2018. After 2018, flood levels decreased again and reached very low levels in 2020 (Figure 2b). Furthermore, both records show that peak flooding occurs during the middle of the year, while the lowest flood levels occur around the turn of the year (December and January). This time pattern is confirmed by a wetlands index (NDWI normalized difference water index), measured by MODIS (not shown).

Both seasonal and interannual variation in flood levels are roughly tracked by area burned. Generally burned area tends to be large following a year with comparably low maximum water level. There are more years with high burned area pre-2011 compared to 2012 to 2019. Water levels returned to low values in

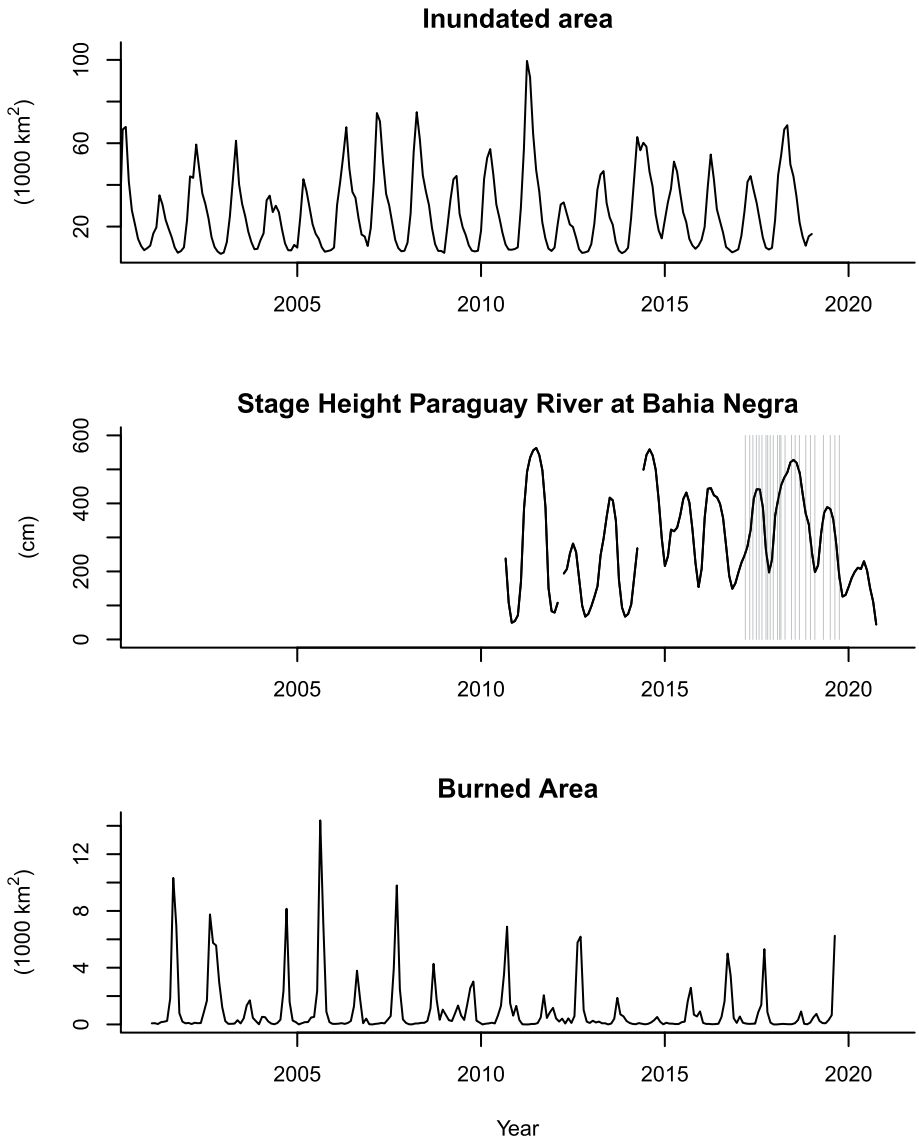

Figure 2. Flooded area estimates for the Pantanal region estimated using remote sensing (Global Inundation Extent from Multisatellites (GIEMS), Prigent et al., 2020) (top panel), Paraguay River stage height at Bahia Negra (middle panel), burned area in the Pantanal region estimated by MODIS (Moderate resolution Imaging Spectroradiometer) on Terra and Aqua satellite missions (Boschetti et al., 2019; Giglio et al., 2018) (lower panel). The vertical lines in the middle panel indicate the dates when vertical profile measurements were made.

2020 when fire frequency and extent have increased to very high levels (not visible in Figure 2c because the record ends in December 2019). In 2020 around 30% of the entire Pantanal area burned (e.g., Mega, 2020). Fires in the Pantanal are predominantly human-caused (e.g., Vigano et al., 2018).

As mentioned above, the difference of PBL mean CH_4 and free troposphere CH_4 indicates the existence and to some extent magnitude of surface-atmosphere fluxes. Vertical profiles do indeed show pronounced elevations in the PBL compared to the free troposphere (Figure 3). The PBL-free troposphere differences reveal a strong seasonality, with flux from the Pantanal to the atmosphere starting just after flood levels have reached their lowest levels. According to PBL-free troposphere differences fluxes increase rapidly during the rise of the water levels, decrease toward the end of the rise and remain low after maximum water levels have been reached (e.g., during peak flood in mid-2018 onwards and similarly from July 2019 onwards). The CH_4 fluxes are not caused by fires as the high CO levels precede high CH_4 values (Figure 3c). The high CO levels are the result of biomass burning and thus indicate the onset and end of the burning season. This is confirmed

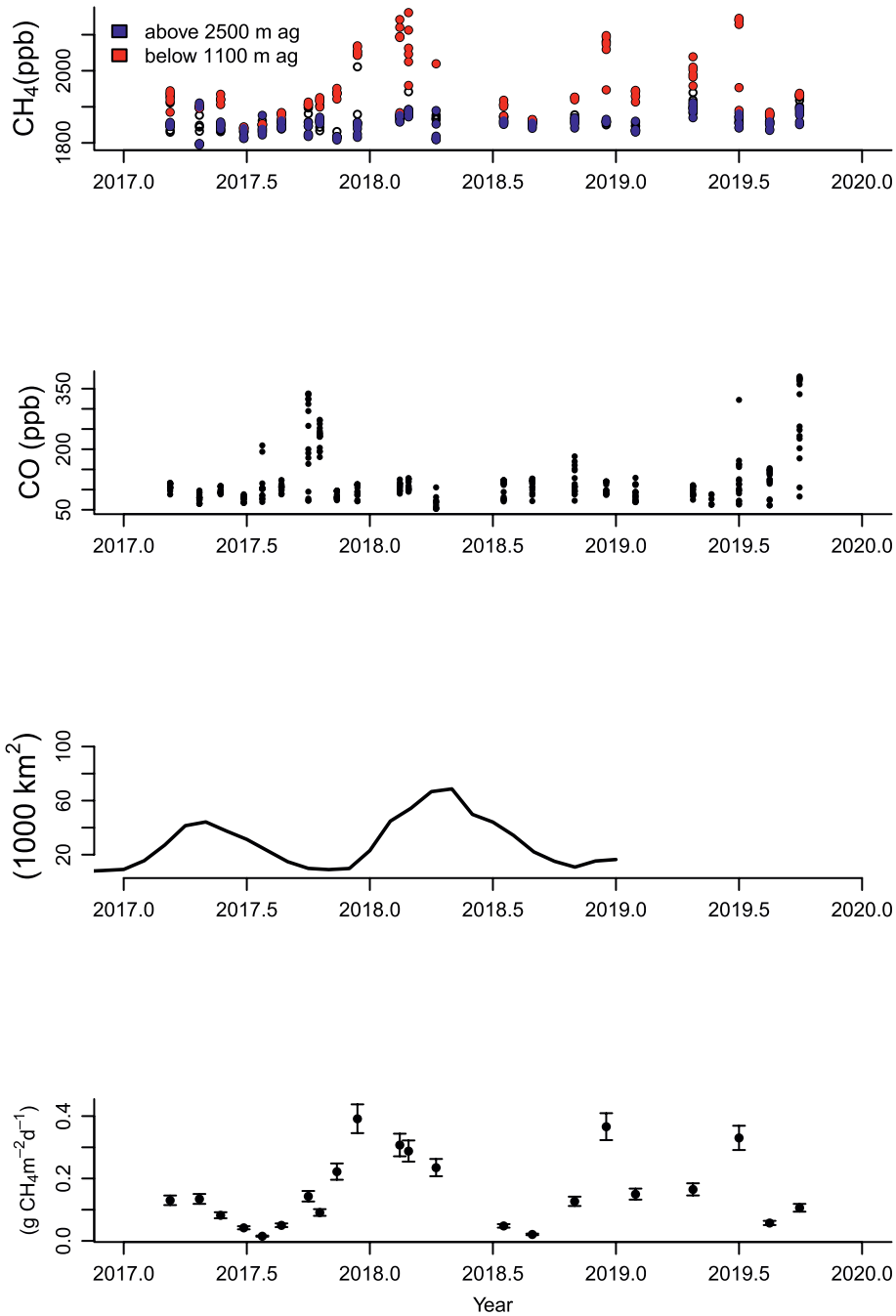

Figure 3. CH_4 dry air mole fraction vertical profiles separated into above and below planetary boundary layer (PBL) height data (top panel) and CO vertical profile data measured above the center of the Pantanal (upper midpanel), inundated area estimated using remote sensing (Global Inundation Extent from Multisatellites [GIEMS], Prigent et al., 2020) (lower mid panel), and CH_4 flux estimates derived using the boundary layer budgeting approach described in the main text (lowest panel).

by coincident timing, and agreement of interannual variation, of a longer time series of air-column CO estimated by MOPITT (Measurement of Pollution in the Troposphere, Deeter, 2013) on the Terra satellite with the burned area time series in Figure 2c (not shown). There is likely a small contribution to CH_4 flux estimates from cattle ranching (estimated as 7.4 $mgCH_4\ m^{-2}\ d^{-1}$ by the EDGAR—Emissions Database for Global Atmospheric Research, greenhouse flux compilation, Crippa et al., 2019). The time-evolution of the

fluxes estimated based on the atmospheric CH_4 vertical profiles suggests that a large flux of CH_4 is emitted during the early ascending phase of water levels during the end of 2017 and early 2018.

As mentioned above, we estimate CH_4 fluxes in two ways. Our first approach based on PBL-free troposphere differences is applicable if these differences are caused by fluxes from the region in question. Back-trajectories calculated for each measurement of a profile during the first year of measurements indicate that air masses have indeed not crossed other major CH_4 emission regions, like Amazonia or Llanos de Moxos, and that air masses travel mostly in the lower troposphere in the surroundings of the Pantanal (Figure S3). To integrate fluxes spatially we assume that they occur spatially homogeneously over Pantanal's flooded area. We thus multiply our flux estimates (interpolated to monthly values) with monthly flooded area estimates of Prigent et al. (2020). We do this for the overlap period of flooded area estimates and CH_4 flux estimates derived from vertical CH_4 profiles (2017–2018). We obtain emissions estimates ranging between 2.0 and 2.8 $TgCH_4\ yr^{-1}$ for mean PBL wind speeds ranging between 10 and 15 $m\ s^{-1}$, respectively (estimated from air-mass trajectories) with fluxes varying between 0 and 0.4 $gCH_4\ m^{-2}\ d^{-1}$. In contrast, the flux estimate estimated by the 3-D atmospheric transport inversion for the entire Pantanal grid cell is $3.5 \pm 3.5\ TgCH_4\ yr^{-1}$ (Figure S1 and Table S1).

4. Discussion

In the following, we first compare the observed Pantanal PBL-free troposphere differences with equivalent values measured above other large-scale wetlands as an indicator of Pantanal flux strength compared to other regions. We then discuss the flux time series relative to water levels revealed by our data and what may determine the observed time course. In order to confirm what our vertical profile data reveal about flux time course we compare them with whole air-column retrievals based on remote sensing which also permits an assessment of the flux strength versus flooded area relationship. Finally, we compare interannual variation and seasonality of fluxes based on our analysis with a widely used global prognostic wetland CH_4 emissions model.

Our vertical profile data reveal episodically large PBL-free troposphere CH_4 differences of up to 300 ppb. For wetlands these are comparably very large enhancements. For comparison, enhancements at two sites in the western/central Amazonia, Rio Branco and Tabatinga, Brazil (Figure 1a), where regular vertical profiles have been measured by LAGEE on a regular basis since 2010, reach enhancement levels up to ~120 ppb (Figure S5). PBL-free troposphere CH_4 differences at Santarem, where profiles have been measured since 2000 (Basso et al., 2016; Miller et al., 2007) (Figure S5), are larger, up to 160 ppb, but nonetheless still substantially smaller compared to Pantanal. Rio Branco and Tabatinga data are expected to sample a somewhat diffuse signal of CH_4 emissions from large seasonally flooded areas to the east of the sites (e.g., Figure 1 in Gatti et al., 2014) while the nature of the source causing the comparably large PBL-free troposphere differences at the Santarem site are not fully understood. These three records reveal also a seasonal cycle suggesting a role played by the Amazon flood pulse. According to Pangala et al. (2017) at these sites emissions via tree stems living in floodplains, functioning as ducts during the seasonal flood, and emissions from open surfaces contribute approximately equally to the total flux. One region where similarly large but temporally less coherent PBL-free troposphere differences compared to the Pantanal have been measured are the West Siberian lowland wetlands (Sasakawa et al., 2017), a vast waterlogged area located between the Ural Mountains (approximately 60°E) and the Jenissey River (approximately 90°E).

A second interesting feature suggested by the Pantanal measurements is that methane seems to be released in large amounts once the minimum flood levels have passed and levels are increasing again. Emissions start to decrease before maximum flood levels have been reached. To confirm these CH_4 release dynamics, as well as to confirm that the measured CH_4 elevations are caused by Pantanal emissions (i.e., differ distinctly from background air), we compared remote sensing-based retrievals from GOSAT for the Pantanal with two reference regions: Brasilia (Mato Grosso), located to the north-east of the Pantanal, and Gran Chaco, located to the south-west (Figure 4). These comparisons do also suggest a quite sudden onset of CH_4 emissions with this occurring just after flood levels have reached their minimum and that maximum emissions precede maximum inundated area (see also Figure S6 which further supports these dynamics). Particularly sharp increases occur in 2011, 2015, and 2017. As an aside, since the enhancements and their variation in

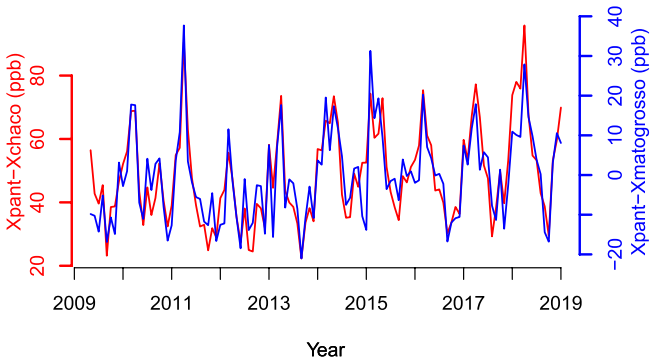

Figure 4. Difference of whole column CH_4 (ppb) at Pantanal and Mato Grosso (north-east of Pantanal, blue line), and Chaco (south-west of Pantanal, red line), respectively, retrieved from shortwave infrared radiances measured on the GOSAT satellite mission.

time are similar when we use a reference located north-east from the Pantanal and a reference located south-east, the air-column CH_4 enhancements (compared to the reference) must indeed be caused by emissions from the Pantanal and not advected from far remote regions in South America like, for example, the Amazon (see also Figure S3).

The reason for the large, quite sudden CH_4 release during low water levels and decrease of flux before reaching maximum flood level is not clear. The CH_4 build-up may be related to transport of fresh decomposable organic matter via the waters from the highlands feeding the Pantanal, which provide substrate for methanogenic bacteria and may also determine the time course of respiration of organic matter and thus oxygen levels in water (Hamilton et al., 1995). Hamilton et al. (1997) indeed demonstrate that oxygen levels in the Paraguay River decrease to very low values during the rising stages of the water, while oxygen levels rapidly rise during the fall of stage levels (their Figure 5). This suggests that depletion of the organic matter pool provided by transport from the "catchment" (or in the rivers themselves) of the river by respiration and methanogenesis takes two to three months. The timing of methane release may also be related, in part, to comparably short gas bubble pathways through the water column and comparably low hydrostatic pressure during initial phase of water-level rise. Direct measurements (Enns et al., 1964) show that saturation pressure of dissolved gases in water increases with pressure, e.g., in the oceans with depth, as a result of increasing hydrostatic pressure, in agreement with predictions of thermodynamics. Several studies observed differences in CH_4 ebullition rates depending on water depth above sediments where methane was formed and atmospheric pressure (e.g., Keller & Stallard, 1994; Mattson & Likens, 1990). The explanation for this phenomenon may be that saturation partial pressure increases with total pressure (sum of atmospheric pressure and hydrostatic pressure of the water column) and that the process of forming a gas bubble involves work against external pressure and surface tension (Figure 5).

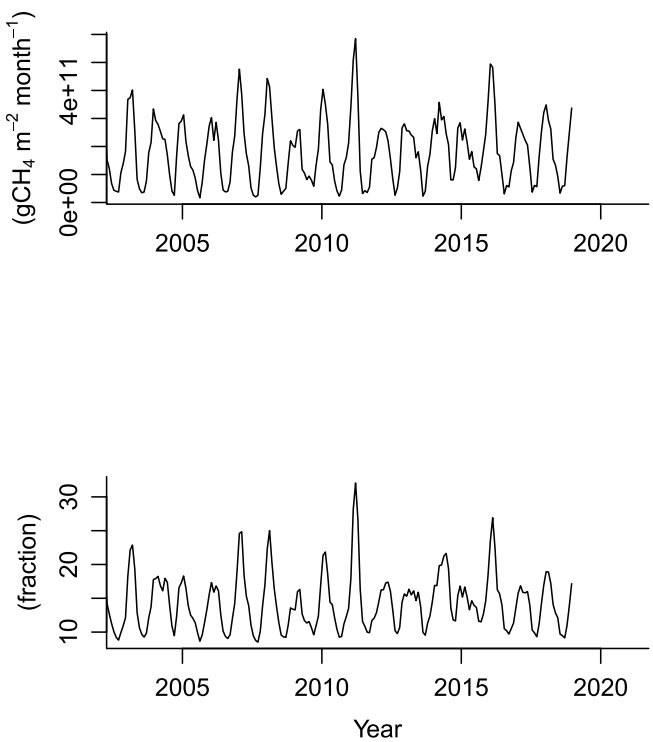

Figure 5. Pantanal average CH_4 flux (upper panel) and fraction of flooded area (lower panel) estimated by LPJ-wsl wetlands model (Zhang et al., 2016).

Our vertical CH_4 profile sampling occurred during a medium to wet period with high water levels in 2018 (Figure 2). Whole-air-column CH_4 retrievals using remote sensing which cover a longer time period can give some indication how CH_4 emissions vary during wetter versus drier years (Figure 4). These data suggest that CH_4 emissions are larger during wetter years. For example, in 2012, a year with low water levels, air-column CH_4 signals are substantially smaller compared to the high water-level year in 2018.

How do our results compare with independent estimates for the Pantanal, other natural CH_4 sources in South America and more generally other wetlands? The total CH_4 emissions estimated based on our approach exploiting PBL-free troposphere differences are somewhat smaller than 3.3 $TgCH_4$ (±30% uncertainty estimated from data in their figures) net annual CH_4 emissions from the Pantanal estimated by Marani and Alvala (2007) using flux chambers and an annual mean flooded area estimated based on river stage levels. They are also smaller than an estimate of Melack et al. (2004) (also 3.3 $TgCH_4\ yr^{-1}$), who multiplied CH_4 flux estimates from Amazonia with flooded area estimates. The uncertainty of this latter estimate is likely of similar order as the Marani and Alvala estimate.

We may also compare these values with estimates of CH_4 emissions from Amazonia. Recent converging estimates both from global atmospheric transport inverse modeling approaches, similar to the one described here, and a large set of surface flux measurements scaled up to the Amazon basin are ~35–50 $TgCH_4\ yr^{-1}$ (Pangala et al., 2017; Ringeval, 2014;

Tunnicliffe et al., 2020; Wilson et al., 2016, 2020), approximately 25–30% of global wetland emissions of ~180 $TgCH_4$ yr^{-1} (Saunois et al., 2016, 2020). Depending on the method used, the CH_4 emissions from the Pantanal are thus on the order of 4–8% of Amazon River catchment CH_4 emissions. Based on synthetic aperture radar data measured from space (Hess et al., 2015), the Amazonian wetlands area is estimated to be ~8.4×10^5 km^2 with flooded fraction of this area varying between 34% and 75%. In percentage terms, the Pantanal maximum inundated area to Amazonia maximum inundated area ratio is thus on the order of 10%.

It is of interest to compare our results with wetland CH_4 emission model predictions as this may possibly suggest further improvements. Comparison with the LPJ-wsl model 2018 version predictions and JULES (not shown) reveal the following. Both models predict a seasonality with flux magnitude of peak fluxes similar to our estimates. The total annual flux predicted by the LPJ-wsl model for September 2017 to August 2018 is 2.2 $TgCH_4$ yr^{-1} (region used to estimate total flux: 24°S to 18°S, and 60°W to 55°W, respectively). This estimate is at the lower end of the results based on the atmospheric approaches. The seasonality of fluxes of LPJ-wsl is highly correlated with water levels with no lags between the two. Thus, this model does not reproduce the observed several months phase shift between maximum fluxes and maximum water levels. Comparison of the LPJ-wsl model predictions of flooded area with Figure 2a furthermore shows that interannual variability of flood levels is captured to some extent (as mentioned earlier and also confirmed by NDWI estimates of flooded area based on data measured by MODIS on satellites). This is likely the result of overland flow not being yet well represented in these models (for the reasons explained above).

Finally, we discuss the pros and cons of our vertical profile troposphere greenhouse gas sampling approach. A main value is that it reveals clearly the seasonality of fluxes. If extended over several years, it will add to our understanding of the cause of interannual variation and thus refine our understanding of controls, and potential future feedbacks. This aspect of our approach distinguishes it from one-off campaigns. It adds to on-the-ground direct flux measurements of Marani and Alvala (2007) for the Pantanal, or Pangala et al. (2017), Melack et al. (2004), and Barbosa et al. (2020) for Amazonia in that the seasonality of the fluxes come out clearly. Our approach focusing on PBL-free troposphere differences is suited for well-localized flux regions. It could be made more precise by measuring PBL-free troposphere exchange time rate e.g., using additional tracers such as O_3 or ^{222}Rn although at some cost (see e.g., Chou et al., 2002). The vertical greenhouse gas profile data can of course also be used in atmospheric transport inversions of Eulerian models (as in this study), as well as Lagrangian models (e.g., Lin et al., 2003; Miller et al., 2007).

5. Summary

We have reported on CH_4 emission estimates from the Pantanal, the largest tropical seasonally flooded savannah. The estimates are based on approximately monthly measured vertical profiles of dry air molar fraction CH_4 vertical profile measurements in the center of the Pantanal from near the ground to approximately 4.5 km height asl, large-scale gradients and inundated area estimated using remote sensing. The data cover the period from March 2017 to September 2019. According to inundated area estimates from remote sensing (Prigent et al., 2020) and river stage records, 2017 was an average year while 2018 was a comparatively wet year. This is also confirmed by burned area records. Flux estimates based on a PBL budgeting technique suggest an annual flux on the order of 2.0–2.8 $TgCH_4$ yr^{-1} for 2017 and 2018 while an atmospheric inverse modeling approach using the CH_4 profile data suggest annual emissions on the order of 3.5 $TgCH_4$ yr^{-1}. This latter estimate is similar to estimates obtained using flux chambers (Marani & Alvala, 2007). Our data indicate an interesting seasonality of CH_4 emissions which start to rise after water levels have reached their lowest level and halt once maximum water levels have been reached. This dynamic is not reproduced by prognostic wetland CH_4 models we used in this study. These models also do not reproduce interannual variation all that well. Our approach—long-term measurement of lower troposphere greenhouse gas vertical profiles—is attractive for revealing seasonal and longer-term trends which may reveal more clearly sensitivity of wetland CH_4 emissions to changes in climate.

Data Availability Statement

CH_4 profile data can be obtained from the NERC (Natural Environmental Research Council) data archive Centre for Environmental Data Analysis (CEDA) via the link https://catalogue.ceda.ac.uk/uuid/d309a5ab60b04b6c82eca6d006350ae6.The latest version of the University of Leicester GOSAT Proxy v9.0 XCH4 data are available from the CEDA data repository at https://doi.org/10.5285/18ef8247f52a4cb6a14013f8235cc1eb (Parker et al., 2020). The version 7.2 used in this study is available from the Copernicus C3S Climate Data Store at https://cds.climate.copernicus.eu.

Acknowledgments
We thank John Melack for an insightful and helpful review. We also thank data providers for this study which include the Brazilian hydrological service, the AQUA, TERRA, and GOSAT remote sensing missions. The GOSAT data were provided the Japanese Aerospace Exploration Agency, National Institute for Environmental Studies and the Ministry of Environment for the GOSAT. We also thank the ALICE High Performance Computing Facility at the University of Leicester for the GOSAT retrievals. We thank Bruno l'Advocaat for help with obtaining river discharge data and Euan Nisbet for leading the NERC MOYA CH_4 consortium from which this study has arisen. Funding for CW, MPC, LVG, LB, and EG has come from MOYA NERC Grant NE/N015657/1, NCEO, and CSSP Brazil. RJP and HB are funded via the UK National Centre for Earth Observation (NE/R016518/1 and NE/N018079/1). LSB is funded by FAPESP (2018/14006-4 and 2019/23654-2). We also acknowledge funding from the ESA GHG-CCI and Copernicus C3S projects.

References

Alho, C. J. R., & Sabino, J. (2012). Seasonal Pantanal flood pulse: Implications for biodiversity conservation—A review. *Oecologia Australis*, *16*, 958–978. https://doi.org/10.4257/oeco.2012.1604.17

Assine, M. L., & Soares, P. C. (2004). Quaternary of the Pantanal, west-central Brazil. *Quaternary International*, *114*, 23–34. https://doi.org/10.1016/s1040-6182(03)00039-9

Baker-Blocker, A., Donahue, T. M., & Mancy, K. H. (1977). Methane flux from wetlands areas. *Tellus*, *29*(3), 245–250. https://doi.org/10.3402/tellusa.v29i3.11353

Barbosa, P. M., Melack, J. M., Amaral, J. H. F., MacIntyre, S., Kasper, D., Cortes, A. C., et al. (2020). Dissolved CH_4 concentrations and fluxes to the atmosphere from a tropical floodplain lake. *Biogeochemistry*, *148*, 129–151. https://doi.org/10.1007/s10533-020-00650-1

Barichivich, J., Gloor, E., Peylin, P., Brienen, R., Schoengart, J., Espinoza, J. C., & Pattnayak, K. C. (2018). Recent intensification of Amazon flooding extremes driven by strengthened Walker circulation. *Science Advances*, *4*, eaat8785. https://doi.org/10.1126/sciadv.aat8785

Basso, L. S., Gatti, L. V., Gloor, M., Miller, J. B., Domingues, L. G., Correia, C. S. C., & Borges, V. F. (2016). Seasonality and Inter-annual variability of CH_4 flux from Eastern Amazon Basin inferred from atmospheric concentration profiles. *Journal of Geophysical Research: Atmospheres*, *121*, 168–184. https://doi.org/10.1002/2015JD023874

Beven, K. J., & Kirkby, M. J. (1979). A physically-based variable contributing area model of basin hydrology. *Hydrological Sciences Bulletin*, *24*(1), 43–69. https://doi.org/10.1080/02626667909491834

Boschetti, L., Roy, D. P., Giglio, L., Huang, H., Zubkova, M., & Humber, M. L. (2019). Global validation of the collection 6 MODIS burned area product. *Remote Sensing of Environment*, *235*, 111490. https://doi.org/10.1016/j.rse.2019.111490

Bridgham, S. D., Cadillo-Quiroz, H., Keller, J. K., & Zhuang, Q. (2013). Methane emissions from wetlands: Biogeochemical, microbial, and modeling perspectives from local to global scales. *Global Change Biology*, *19*, 1325–1346. https://doi.org/10.1111/gcb.12131

Chipperfield, M. P. (2006). New version of the TOMCAT/SLIMCAT offline chemical transport model: Intercomparison of stratospheric tracer experiments. *Quarterly Journal of the Royal Meteorological Society*, *132*, 1179–1203. https://doi.org/10.1256/qj.05.51

Chou, W. W., Wofsy, S. C., Harriss, R. C., Lin, J. C., Gerbig, C., & Sachse, G. W. (2002). Net fluxes of CO_2 in Amazonia derived from aircraft observations. *Journal of Geophysical Research*, *107*(D22), 4614. https://doi.org/10.1029/2001JD001295

Cicerone, R. J., & Oremland, R. S. (1988). Biogeochemical aspects of atmospheric methane. *Global Biogeochemical Cycles*, *2*(4), 299–327. https://doi.org/10.1029/GB002i004p00299

Crippa, M., Solazzo, E., Huang, G., Guizzardi, D., Koffi, E., Muntean, M., et al. (2019). High resolution temporal profiles in the Emissions Database for Global Atmospheric Research (EDGAR). *Nature Scientific Data*, *7*, 121. https://doi.org/10.1038/s41597-020-0462-2

Deeter, M. N. (2013). *MOPITT (Measurements of Pollution in the Troposphere) version 6. Product user's guide*. Boulder, CO: National Center for Atmospheric Research.

Diegues, A. C. S. (Ed.), (1994). *An inventory of Brazilian wetlands*. Gland, Switzerland: IUCN.

Dlugokencky, E. J., Masarie, K. A., Lang, P. M., & Tans, P. P. (1998). Continuing decline in the growth rate of the atmospheric methane burden. *Nature*, *393*, 447–450. https://doi.org/10.1038/30934

Enns, T., Scholander, P. F., & Bradstreet, E. D. (1964). Effect of hydrostatic pressure on gases dissolved in water. *The Journal of Physical Chemistry*, *69*(2), 389–391.

Evans, T. L., Costa, M., Tomas, W. M., & Camilo, A. R. (2014). Large-scale habitat mapping of the Brazilian Pantanal wetland: A synthetic aperture radar approach. *Remote Sensing of Environment*, *155*, 89–108. https://doi.org/10.1016/j.rse.2013.08.051

Frankenberg, C., Platt, U., & Wagner, T. (2005). Iterative maximum a posteriori (IMAP)-DOAS for retrieval of strongly absorbing trace gases: Model studies for CH_4 and CO_2 retrieval from near infrared spectra of SCIAMACHY onboard ENVISAT. *Atmospheric Chemistry and Physics*, *5*, 9–22. https://doi.org/10.5194/acp-5-9-2005

Gatti, L. V., Gloor, M., Miller, J. B., Doughty, C. E., Malhi, Y., Domingues, L. G., et al. (2014). Drought sensitivity of Amazonian carbon balance revealed by atmospheric measurements. *Nature*, *506*, 76–80. https://doi.org/10.1038/nature12957

Gedney, N., & Cox, P. M. (2003). The sensitivity of global climate model simulations to the representation of soil moisture heterogeneity. *Journal of Hydrometeorology*, *4*, 1265–1275. https://doi.org/10.1175/1525-7541(2003)004<1265:TSOGCM>2.0.CO;2

Gelaro, R., McCarty, W., Suárez, M. J., Todling, R., Molod, A., Takacs, L., et al. (2017). The modern-era retrospective analysis for research and applications, Version 2 (MERRA-2). *Journal of Climate*, *30*, 5419–5454. https://doi.org/10.1175/JCLI-D-16-0758.1

Giglio, L., Boschetti, L., Roy, D. P., Humber, M. L., & Justice, C. O. (2018). The Collection 6 MODIS burned area mapping algorithm and product. *Remote Sensing of Environment*, *217*, 72–85. https://doi.org/10.1016/j.rse.2018.08.005

Gloor, E., Wilson, C., Chipperfield, M. P., Chevallier, F., Buermann, W., Boesch, H., et al. (2018). Tropical land carbon cycle responses to 2015/16 El Niño as recorded by atmospheric greenhouse gas and remote sensing data. *Philosophical Transactions of the Royal Society B*, *373*, 20170302. https://doi.org/10.1098/rstb.2017.0302

Hamilton, S., Sippel, S., & Melack, J. M. (1995). Oxygen depletion and carbon dioxide and methane production in waters of the Pantanal wetland of Brazil. *Biogeochemistry*, *30*, 115–141. https://doi.org/10.1007/BF00002727

Hamilton, S. K., Sippel, S., Calheiros, D. F., & Melack, J. M. (1997). An anoxic event and other biogeochemical effects of the Pantanal wetland on the Paraguay River. *Limnology & Oceanography*, *42*, 257–272. https://doi.org/10.4319/lo.1997.42.2.0257

Hamilton, S. K., Sippel, S. J., & Melack, J. M. (2002). Comparison of inundation patterns among major South American floodplains. *Journal of Geophysical Research*, *107*(D20), 8038. https://doi.org/10.1029/2000JD000306

Hess, L. L., Melack, J. M., Affonso, A. G., Barbosa, C., Gastil-Buhl, M., & Novo, E. M. L. M. (2015). Wetlands of the Lowland Amazon Basin: Extent, Vegetative Cover, and Dual-season Inundated Area as Mapped with JERS-1 Synthetic Aperture Radar. *Wetlands*, *35*, 745–756. https://doi.org/10.1007/s13157-015-0666-y

IPCC. (2014). In R. K. Pachauri, & L. A. Meyer (Eds.), *Climate change (2014). Synthesis report. Contribution of working Groups I, II and III to the Fifth assessment report of the Intergovernmental panel on climate change, Core writing team*. Geneva, Switzerland: IPCC.

Ivory, S. J., McGlue, M. M., Spera, S., Silva, A., & Bergier, I. (2019). Vegetation, rainfall, and pulsing hydrology in the Pantanal, the world's largest tropical wetland. *Environmental Research Letters*, *14*, 124017. https://doi.org/10.1088/1748-9326/ab4ffe

Jiménez-Muñoz, J. C., Sobrino, J. A., Mattar, C., & Malhi, Y. (2013). Spatial and temporal patterns of the recent warming of the Amazon forest. *Journal of Geophysical Research: Atmospheres*, *118*, 5204–5215. https://doi.org/10.1002/jgrd.50456

Junk, W. J., Piedade, M. T. F., Lourival, R., Wittmann, F., Kandus, P., Lacerda, L. D., et al. (2014). Brazilian wetlands: Their definition, delineation, and classification for research, sustainable management, and protection. *Aquatic Conservation: Marine and Freshwater Ecosystems*, *24*, 5–22. https://doi.org/10.1002/aqc.2386

Keddy, P. A., Fraser, L. H., Solomeshch, A. I., Junk, W. J., Campbell, D. R., Arroyo, M. T. K., & Alho, C. J. R. (2009). Wet and wonderful: The world's largest wetlands are conservation priorities. *BioScience*, *59*(1), 39–51. https://doi.org/10.1525/bio.2009.59.1.8

Keller, M., & Stallard, R. F. (1994). Methane emissions by bubbling from Gatun Lake, Panama. *Journal of Geophysical Research*, *99*, 8307–8319. https://doi.org/10.1029/92JD02170

Kuze, A., Suto, H., Nakajima, M., & Hamazaki, T. (2009). Thermal and near infrared sensor for carbon observation Fourier-transform spectrometer on the Greenhouse Gases Observing Satellite for greenhouse gases monitoring. *Applied Optics*, *48*(35), 6716–6733. https://doi.org/10.1364/ao.48.006716

Levy, H., II. (1971). Normal atmosphere: Large radical and formaldehyde concentrations predicted. *Science*, *173*, 141–143. https://doi.org/10.1126/science.173.3992.141

Lin, J. C., Gerbig, C., Wofsy, S. C., Andrews, A. E., Daube, B. C., Davis, K. J., & Grainger, C. A. (2003). A near-field tool for simulating the upstream influence of atmospheric observations: The Stochastic Time-Inverted Lagrangian Transport (STILT) model. *Journal of Geophysical Research*, *108*(D16), 4493–4501. https://doi.org/10.1029/2002JD003161

MacFarling Meure, C., Etheridge, D., Trudinger, C., Steele, P., Langenfelds, R., van Ommen, T., et al. (2006). The law dome CO_2, CH_4 and N_2O ice core records extended to 2000 years BP. *Geophysical Research Letters*, *33*, L14810. https://doi.org/10.1029/2006GL026152

Marani, L., & Alvala, P. C. (2007). Methane emissions from lakes and floodplains in Pantanal, Brazil. *Atmospheric Environment*, *41*, 1627–1633. https://doi.org/10.1016/j.atmosenv.2006.10.046

Mattson, M. D., & Likens, G. E. (1990). Air pressure and methane fluxes. *Nature*, *347*, 718–719. https://doi.org/10.1038/347718b0

McNorton, J., Gloor, E., Wilson, C., Hayman, G. D., Gedney, N., Comyn-Platt, E., et al. (2016). Role of regional wetland emissions in atmospheric methane variability. *Geophysical Research Letters*, *43*, 11433–11444. https://doi.org/10.1002/2016GL070649

Mega, E. R. (2020). Apocalyptic' fires ravaging the world's largest tropical wetland. *Nature*, *586*, 20–21. https://doi.org/10.1038/d41586-020-02716-4

Melack, J. M., Hess, L. L., Gastil, M., Forsberg, B. R., Hamilton, S. K., Lima, I. B. T., & Novo, E. M. L. M. (2004). Regionalization of methane emissions in the Amazon Basin with microwave remote sensing. *Global Change Biology*, *10*, 530–544. https://doi.org/10.1111/j.1529-8817.2003.00763.x10.1111/j.1365-2486.2004.00763.x

Miller, J. B., Gatti, L. V., d'Amelio, M. T. S., Crotwell, A. M., Dlugokencky, E. J., Bakwin, P., et al. (2007). Airborne measurements indicate large methane emissions from the eastern Amazon basin. *Geophysical Research Letters*, *34*, L10809. https://doi.org/10.1029/2006GL029213

Monks, S. A., Wilson, C., Emmons, L. K., Hannigan, J. W., Helmig, D., Blake, N. J., & Blake, D. R. (2018). Using an inverse model to reconcile differences in simulated and observed global ethane concentrations and trends between 2008 and 2014. *Journal of Geophysical Research: Atmospheres*, *123*, 11262–11282. https://doi.org/10.1029/2017JD028112

Nisbet, E. G., Dlugokencky, E. J., Manning, M. R., Lowry, D., Fisher, R. E., France, J. L., et al. (2016). Rising atmospheric methane: 2007–2014 growth and isotopic shift. *Global Biogeochemical Cycles*, *30*, 1356–1370. https://doi.org/10.1002/2016GB005406

Ovando, A., Tomasella, J., Rodriguez, D. A., Martinez, J. M., Siqueira-Junior, J. L., Pinto, G. L. N., et al. (2015). Extreme flood events in the Bolivian Amazon wetlands. *Journal of Hydrology: Regional Studies*, *5*, 293–308.

Pangala, R. S., Enrich-Prast, A., Basso, L. S., Bittencourt Peixoto, R., Bastviken, D., Hornibrook, E. R. C., et al. (2017). Large emissions from floodplain trees close the Amazon methane budget. *Nature*, *552*, 230–234. https://doi.org/10.1038/nature24639

Parker, R., Boesch, H., Cogan, A., Fraser, A., Feng, L., Palmer, P. I., et al. (2011). Methane observations from the Greenhouse Gases Observing SATellite: Comparison to ground-based TCCON data and model calculations. *Geophysical Research Letters*, *38*, L15807. https://doi.org/10.1029/2011GL047871

Parker, R. J., Boesch, H., McNorton, J., Comyn-Platt, E., Gloor, M., Wilson, C., et al. (2018). Evaluating year-to-year anomalies in tropical wetland methane emissions using satellite CH_4 observations. *Remote Sensing of Environment*, *211*, 261–275. https://doi.org/10.1016/j.rse.2018.02.011

Parker, R. J., Webb, A., Boesch, H., Somkuti, P., Barrio Guillo, R., Di Noia, A., et al. (2020). A decade of GOSAT proxy satellite CH_4 observations. *Earth System Science Data*, *12*, 3383–3412. https://doi.org/10.5194/essd-12-3383-2020

Prigent, C., Jimenez, C., & Bousquet, P. (2020). Satellite-derived global surface water extent and dynamics over the last 25 years (GIEMS-2). *Journal of Geophysical Research: Atmospheres*, *125*, e2019JD030711. https://doi.org/10.1029/2019JD030711

Ringeval, B., Houweling, S., van Bodegom, P. M., Spahni, R., van Beek, R., Joos, F., & Röckmann, T. (2014). Methane emissions from floodplains in the Amazon Basin: Challenges in developing a process-based model for global applications, *Biogeosciences 11*, 1519–1558. https://doi.org/10.5194/bg-11-1519-2014

Sasakawa, M., Machida, T., Ishijima, K., Arshinov, M., Patra, P. K., Ito, A., et al. (2017). Temporal characteristics of CH_4 vertical profiles observed in the West Siberian Lowland over Surgut from 1993 to 2015 and Novosibirsk from 1997 to 2015. *Journal of Geophysical Research: Atmospheres*, *122*, 11261–11273. https://doi.org/10.1002/2017JD026836

Saunois, M., Bousquet, P., Poulter, B., Peregon, A., Ciais, P., Canadell, J. G., et al. (2016). The global methane budget 2000–2012. *Earth System Science Data*, *8*, 697–751. https://doi.org/10.5194/essd-8-697-2016

Saunois, M., Stavert, A. R., Poulter, B., Bousquet, P., Canadell, J. G., Jackson, R. B., et al. (2020). The Global Methane Budget 2000–2017. *Earth System Science Data*, *12*, 1561–1623. https://doi.org/10.5194/essd-12-1561-2020

Schulz, C., Whitney, B. S., Rossetto, O. C., Neves, D. M., Crabb, L., Castro de Oliveira, E., et al. (2019). Physical, ecological and human dimensions of environmental change in Brazil's Pantanal wetland: Synthesis and research agenda. *The Science of the Total Environment*, *687*, 1011–1027. https://doi.org/10.1016/j.scitotenv.2019.06.023

Sitch, S., Smith, B., Prentice, I. C., Arneth, A., Bondeau, A., Cramer, W., et al. (2003). Evaluation of ecosystem dynamics, plant geography and terrestrial carbon cycling in the LPJ dynamic global vegetation model. *Global Change Biology*, *9*(2), 161–185. https://doi.org/10.1046/j.1365-2486.2003.00569.x

Tunnicliffe, R. L., Ganesan, A. L., Parker, R. J., Boesch, H., Gedney, N., Poulter, B., et al. (2020). Quantifying sources of Brazil's CH_4 emissions between 2010 and 2018 from satellite data. *Atmospheric Chemistry and Physics*, *20*, 13041–13067. https://doi.org/10.5194/acp-20-13041-2020

Vigano, H. H. G., de Souza, C. C., Neto, J. F. R., Cristaldo, M. F., & Jesus, L. D. (2018). Previsão e Modelagem das Ocorrências de Incêndios no Pantanal. *Revista Brasileira de Meteorologia*, *33*(2), 306–316. https://doi.org/10.1590/0102-7786332012

Webb, A. J., Bösch, H., Parker, R. J., Gatti, L. V., Gloor, E., Palmer, P. I., et al. (2016). CH_4 concentrations over the Amazon from GOSAT consistent with in situ vertical profile data. *Journal of Geophysical Research: Atmospheres*, *121*, 11006–11020. https://doi.org/10.1002/2016JD025263

Wilson, C., Chipperfield, M. P., Gloor, M., & Chevallier, F. (2014). Development of a variational flux inversion system (INVICAT v1.0) using the TOMCAT chemical transport model. *Geoscientific Model Development*, *7*, 2485–2500. https://doi.org/10.5194/gmd-7-2485-2014

Wilson, C., Chipperfield, M. P., Gloor, M., Parker, R. J., Boesch, H., McNorton, J., et al. (2021). Large and increasing methane emissions from Eastern Amazonia derived from satellite data, 2010–2018. *Atmospheric Chemistry and Physics Discussions*, *21*, 10643–10669. https://doi.org/10.5194/acp-2020-1136]

Wilson, C., Gloor, M., Gatti, L. V., Miller, J. B., Monks, S. A., McNorton, J., et al. (2016). Contribution of regional sources to atmospheric methane over the Amazon Basin in 2010 and 2011. *Global Biogeochemical Cycles*, *30*, 400–420. https://doi.org/10.1002/2015GB005300

Zhang, Z., Zimmermann, N. E., Calle, L., Hurtt, G., Chatterjee, A., & Poulter, B. (2018). Enhanced response of global wetland methane emissions to the 2015–2016 El Niño-Southern Oscillation event. *Environmental Research Letters*, *13*(7), 074009. https://doi.org/10.1088/1748-9326/aac939

Zhang, Z., Zimmermann, N. E., Kaplan, J. O., & Poulter, B. (2016). Modeling spatiotemporal dynamics of global wetlands: Comprehensive evaluation of a new sub-grid TOPMODEL parameterization and uncertainties. *Biogeosciences*, *13*(5), 1387–1408. https://doi.org/10.5194/bg-13-1387-2016

References From the Supporting Information

Chevallier, F., Bréon, F.-M., & Rayner, P. J. (2007). Contribution of the orbiting carbon observatory to the estimation of CO_2 sources and sinks: Theoretical study in a variational data assimilation framework. *Journal of Geophysical Research*, *112*, D09307. https://doi.org/10.1029/2006JD007375

Clark, D. B., Mercado, L. M., Sitch, S., Jones, C. D., Gedney, N., Best, M. J., et al. (2011). The joint UK land environment simulator (JULES), model description—Part 2: Carbon fluxes and vegetation dynamics. *Geoscientific Model Development*, *4*, 701–722. https://doi.org/10.5194/gmd-4-701-2011

Dee, D. P., Uppala, S. M., Simmons, A. J., Berrisford, P., Poli, P., Kobayashi, S., et al. (2011). The ERA-Interim reanalysis: Configuration and performance of the data assimilation system. *Quarterly Journal of the Royal Meteorological Society*, *137*, 553–597. https://doi.org/10.1002/qj.828

Draxler, R. R., & Hess, G. D. (1998). An overview of the HYSPLIT 4 modeling system for trajectories, dispersion, and deposition. *Australian Meteorological Magazine*, *47*(4), 295–308.

Fisher, M., & Courtier, P. (1995). *Estimating the covariance matrices of analysis and forecast errors in variational data assimilation (ECMWF Tech. Memo 220, 28 pp.)*. https://doi.org/10.21957/1dxrasjit

Huijnen, V., Williams, J., van Weele, M., van Noije, T., Krol, M., Dentener, F., et al. (2010). The global chemistry transport model TM5: Description and evaluation of the tropospheric chemistry version 3.0. *Geoscientific Model Development*, *3*, 445–473. https://doi.org/10.5194/gmd-3-445-2010

McNorton, J., Wilson, C., Gloor, M., Parker, R. J., Boesch, H., Feng, W., et al. (2018). Attribution of recent increases in atmospheric methane through 3-D inverse modelling. *Atmospheric Chemistry and Physics*, *18*, 18149–18168. https://doi.org/10.5194/acp-18-18149-2018

Murguia-Flores, F., Arndt, S., Ganesan, A. L., Murray-Tortarolo, G., & Hornibrook, E. R. C. (2018). Soil Methanotrophy Model (MeMo v1.0): A process-based model to quantify global uptake of atmospheric methane by soil. *Geoscientific Model Development*, *11*, 2009–2032. https://doi.org/10.5194/gmd-11-2009-2018

Olivier, J. G. J., & Janssens-Maenhout, G. (2012). *Trends in global CO_2 emissions: 2012 report*. The Hague: PBL Netherlands Environmental Assessment Agency.

Patra, P. K., Houweling, S., Krol, M., Bousquet, P., Belikov, D., Bergmann, D., et al. (2011). TransCom model simulations of CH_4 and related species: Linking transport, surface flux and chemical loss with CH_4 variability in the troposphere and lower stratosphere. *Atmospheric Chemistry and Physics*, *11*, 12813–12837. https://doi.org/10.5194/acp-11-12813-2011

Spivakovsky, C. M., Logan, J. A., Montzka, S. A., Balkanski, Y. J., Foreman-Fowler, M., Jones, D. B. A., et al. (2000). Three-dimensional climatological distribution of tropospheric OH: Update and evaluation. *Journal of Geophysical Research*, *105*, 8931–8980. https://doi.org/10.1029/1999JD901006

Werf, van der G. R., Randerson, J. T., Giglio, L., van Leeuwen, T., Chen, Y., et al. (2017). Global fire emissions estimates during 1997–2016. *Earth System Science Data*, *9*, 697–720. https://doi.org/10.5194/essd-9-697-2017

Yan, X., Akiyama, H., Yagi, K., & Akimoto, H. (2009). Global estimations of the inventory and mitigation potential of methane emissions from rice cultivation conducted using the 2006 Intergovernmental Panel on Climate Change Guidelines. *Global Biogeochemical Cycles*, *23*, GB2002. https://doi.org/10.1029/2008GB003299